AIP | Journal of Applied Physics

Upconversion luminescence in Er3+ doped and Er3+/Yb3+ codoped zirconia and hafnia nanocrystals excited at 980 nm

Luis A. Gómez, Leonardo de S. Menezes, Cid B. de Araújo, Rogeria R. Gonçalves, Sidney J. L. Ribeiro et al.

Citation: J. Appl. Phys. **107**, 113508 (2010); doi: 10.1063/1.3428478
View online: http://dx.doi.org/10.1063/1.3428478
View Table of Contents: http://jap.aip.org/resource/1/JAPIAU/v107/i11
Published by the AIP Publishing LLC.

Upconversion luminescence in Er^{3+} doped and Er^{3+}/Yb^{3+} codoped zirconia and hafnia nanocrystals excited at 980 nm

Luis A. Gómez,[1,a] Leonardo de S. Menezes,[1] Cid B. de Araújo,[1] Rogeria R. Gonçalves,[2] Sidney J. L. Ribeiro,[3] and Younes Messaddeq[3]
[1]*Departamento de Física, Universidade Federal de Pernambuco, 50670-901 Recife-PE, Brazil*
[2]*Departmento de Química, FFCLRP-USP, 14040-90, Ribeirão Preto-SP, Brazil*
[3]*Instituto de Química, UNESP-Univ. Estadual Paulista, 14801-970 Araraquara-SP, Brazil*

(Received 29 December 2009; accepted 15 April 2010; published online 1 June 2010)

Frequency upconversion (UC) luminescence in nanocrystalline zirconia (ZrO_2) and hafnia (HfO_2) doped with Er^{3+} and Yb^{3+} was studied under continuous-wave excitation at 980 nm. Samples of $ZrO_2:Er^{3+}$, $ZrO_2:Er^{3+}/Yb^{3+}$, and $HfO_2:Er^{3+}/Yb^{3+}$ were prepared by the sol-gel technique and characterized using x-ray diffraction and electron microscopy. A study of the infrared-to-green and infrared-to-red UC processes was performed including the analysis of the spectral and the temporal behavior. The mechanisms contributing to the UC luminescence were identified as excited state absorption and energy transfer among rare-earth ions. © *2010 American Institute of Physics*. [doi:10.1063/1.3428478]

I. INTRODUCTION

Dielectric materials doped with rare earth (RE) ions have been attracting large attention due to the possibility of applications in photonic devices.[1,2] In particular, a phenomenon that has been receiving especial attention is the optical frequency upconversion (UC), widely used to obtain visible luminescence using lasers operating in the infrared region for excitation of the samples. Generally, in order to observe efficient UC emissions the host material should have low cutoff phonon frequency to allow large lifetime of the RE ions electronic levels.[3–5] In addition, high UC efficiencies depend on the doping strategy used, like using codopants and/or metallic nanoparticles.[6–8] For some applications, e.g., displays and sensors, nanostructured materials play a relevant role.[9]

An important photonic material for UC studies is zirconia (ZrO_2) which has high refractive index and low phonon cutoff frequency.[10] Previous studies show that ZrO_2 nanocrystals (NC) doped with Er^{3+} or codoped with Er^{3+}/Yb^{3+} under infrared excitation is luminescent at ≈525 nm, ≈550 nm, and ≈650 nm, due to transitions from the Er^{3+} states $^2H_{11/2}$, $^4S_{3/2}$, and $^4F_{9/2}$ to the ground state ($^4I_{15/2}$).[11] Although electronic $4f-4f$ transitions are forbidden for the electric dipole mechanism, this rule is broken when the ion occupies a lattice site without inversion symmetry. In such situation, the local field associated to the crystal structure plays an important role in the luminescence process. In the ZrO_2 case, one observes monoclinic, tetragonal, and cubic phases, and since the first one is the less symmetric, one expects a larger luminescence efficiency when RE ions are hosted in such structure. Moreover, it is observed that for all ZrO_2 phases, the more energetic phonon modes have energies comparable to or smaller than 500 cm^{-1}.[12]

Another system of interest is hafnia (HfO_2), which is a high-K material that is widely used as optical coating. HfO_2 is isostructural with ZrO_2, and when doped with RE it presents similarities in the optical properties.[13,14] In a recent work, Matarelli *et al.*[15] have performed spectroscopic studies (Raman and luminescence) of Er^{3+}-doped HfO_2 NC in silicate glass ceramics obtained by sol-gel-techniques. They could determine also the structure of the grown HfO_2 NC by performing X-ray diffraction (XRD) on the samples.

For both matrices it is observed a transparency window over a wide wavelength range, as well as high refractive index and similar Raman spectra. UC emission at ≈650 nm under excitation at 980 nm was reported for Er^{3+} doped SiO_2-HfO_2 films.[16] However, the UC phenomenon in RE doped HfO_2 NC was not studied before.

In this work, we present a study of the infrared-to-green and infrared-to-red UC processes for NC of ZrO_2 and HfO_2 singly doped with Er^{3+} and codoped by Er^{3+}/Yb^{3+} ions. The luminescence spectra of the samples was analyzed and the mechanisms contributing for the UC processes were identified with basis on the UC signal dependence with laser intensity, RE ions concentration, and the temporal response of the samples.

II. EXPERIMENTAL

ZrO_2 NC were prepared from a suspension of $ZrOCl_2$ (zirconium oxichloride) in ethanol. The mixture of $ZrOCl_2$, ethanol was refluxed for 1 h leading to stable NC suspension. Finally, erbium and ytterbium were added as chloride salts to obtain molar ratios of 0.5% and 1.0% for Er^{3+} and 10.0% for Yb^{3+}.

HfO_2 NC were prepared in the same way from $HfOCl_2$ and ethanol under reflux for 1h to get a fully transparent suspension. The HfO_2 NC suspension was filtered through a 0.2 μm filter and then erbium and ytterbium were added as chloride salts to obtain molar ratios of 1.0% for Er^{3+} and 1.0% for Yb^{3+}.

[a]Author to whom correspondence should be addressed. Present address: Escola Politécnica de Pernambuco—Universidade de Pernambuco, 50750-470 Recife, PE, Brazil. Electronic mail: lagomezma@poli.br.

TABLE I. Characteristics of the studied samples, as well as their compositions (mol %).

Sample	Matrix	Structure	NC average size (nm)	Dopant concentration (mol %)	
				Er^{3+}	Yb^{3+}
A	ZrO_2	Monoclinic	82	0.5	0.0
B	ZrO_2	Monoclinic	71	1.0	0.0
C	ZrO_2	Tetragonal	43	1.0	1.0
D	HfO_2	Monoclinic (dominant) and tetragonal	39	1.0	1.0

All suspensions were dried at room temperature and then annealed at 900 °C during 2 h. As a result of the synthesis procedure fine and homogenous powders are obtained. The preparation of the samples for the optical experiments was made by pressing the powders in a sample holder which allowed maintaining the same excitation and optical signal collection conditions for all samples. The composition and the sizes of the NC, as well as samples' nomenclature, are summarized in Table I.

The crystalline phases of the calcinated powders were identified by analysis of the XRD pattern. Morphology and particle sizes were determined using a transmission electron microscope. Laser excitation was made using a continuous wave (cw) diode laser (~30 mW) operating at 980 nm, which was modulated by a chopper at 288 Hz, located in the focus of a 1:1 telescope. After passing through the telescope, the excitation beam was focused by a 5 cm focal length lens on the samples.

Fluorescence spectra were collected using a multimode optical fiber connected to a monochromator to which a photomultiplier tube with gallium arsenide photocathode was attached. A digital oscilloscope was used to record the UC signals that were obtained with the samples at room temperature. The excitation of the samples and the signal collection were carried out under the same conditions for all samples studied.

III. RESULTS AND DISCUSSION

The XRD patterns are shown in Fig. 1. Monoclinic phase was observed for the zirconia samples doped only with erbium (samples A and B) and tetragonal phase for the sample codoped with Er^{3+}/Yb^{3+} (sample C). The HfO_2 sample codoped with Er^{3+}/Yb^{3+} (sample D) shows tetragonal and monoclinic phases with the latter phase being dominant. A similar result was reported for sol-gel derived HfO_2 films.[17]

Figure 2 shows the emission spectra under cw excitation at 980 nm. Green and red UC emissions are observed at ≈525, ≈550, and ≈650 nm, corresponding to transitions from states $^2H_{11/2}$, $^4S_{3/2}$, and $^4H_{9/2}$ to the Er^{3+} ground state ($^4I_{15/2}$), respectively. It is observed in Fig. 2 that the green emission increases with the Er^{3+} concentration but the red emission remains weak. The relevant energy levels for Er^{3+} and Yb^{3+}, as well as the UC emissions, represented by the solid arrows are shown in Fig. 3. The UC emission in the spectral region from 520 to 570 nm is due to the successive optical transitions $^4I_{15/2} \rightarrow {}^4I_{11/2}$ and $^4I_{11/2} \rightarrow {}^4F_{7/2}$, followed by nonradiative decay to levels $^2H_{11/2}$ and $^4S_{3/2}$. Then, radiative transitions from these levels to the ground state multiplet originate the green emissions. This UC pathway was previously identified for Er^{3+} hosted in different bulk crystals and glasses.[18,19] The red emission is weak because the nonradiative transition $(^2H_{11/2}, {}^4S_{3/2}) \rightarrow {}^4F_{9/2}$ is not efficient, since the energy gap of ~2000 cm^{-1} would require the simultaneous creation of at least four phonons. The excitation pathway can be checked by measuring the dependence of the UC luminescence intensity with the pump power. The results shown in Fig. 4 indicate a slope is ≈2.0 for samples A and B, corresponding to the absorption of two photons.

The excitation pathway in samples C and D is different than in samples A and B due to the presence of Yb^{3+} ions.

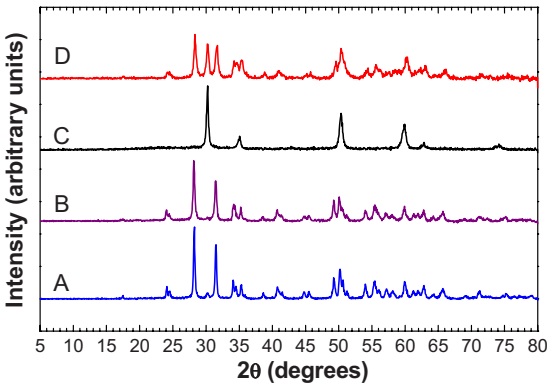

FIG. 1. (Color online) X-ray diffractograms. Samples: A (ZrO_2:Er^{3+} 0.5%), B (ZrO_2:Er^{3+} 1.0%), C (ZrO_2:Er^{3+} 1.0%/Yb^{3+} 1.0%), and D (HfO_2:Er^{3+} 1.0%/Yb^{3+} 1.0%). The data were displaced in the vertical scale for a better visualization.

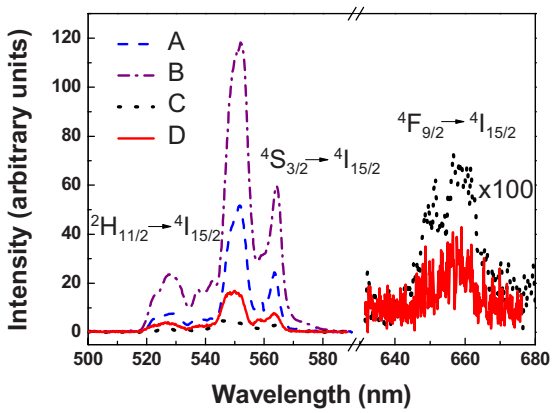

FIG. 2. (Color online) UC spectra emitted by the samples when excited at 980 nm.

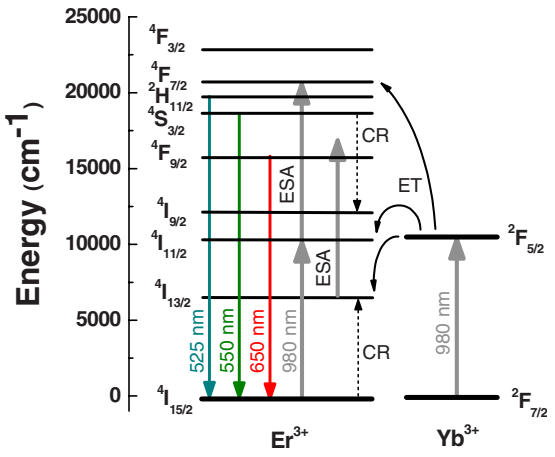

FIG. 3. (Color online) Energy levels scheme for the Er^{3+} and Yb^{3+} ions. The solid arrows represent photons absorbed or emitted by the ions. Dashed and curly arrows represent cross relaxation and ET processes, respectively.

Because the laser wavelength is in resonance with the Yb^{3+} transition $^2F_{5/2} \rightarrow {}^2F_{7/2}$ and because its oscillator strength is greater than the Er^{3+} transition $^4I_{15/2} \rightarrow {}^4I_{11/2}$, the excitation of levels $^2H_{11/2}$ and $^4S_{3/2}$ is mainly due to energy transfer (ET) from Yb^{3+} to Er^{3+} ions. The ET efficiency depends on the relative concentration of Er^{3+} and Yb^{3+} and the lifetime of the levels participating in the process. Because the trivalent RE ions substitute tetravalent Zr^{4+} and Hf^{4+} and because of the higher concentration in samples C and D, the ET between Yb^{3+} and Er^{3+} ions may be efficient and thus the Er^{3+} levels' lifetimes may change by large amount in comparison with samples A and B. Moreover, clusters of Yb^{3+} and Er^{3+} ions can be formed due to charge compensation.

To obtain a better understanding of the UC behavior the time evolution of the luminescence signal was investigated chopping the laser beam. The results shown in Figs. 5 and 6 are summarized in Table II. A reference signal proportional to the laser intensity is presented in both figures to indicate the smallest rise-time and decay-time that could be measured after the interruption of the excitation laser by the chopper. The characteristic times given in Table II were determined using a simple exponential function matched between 33% and 1%, and 67% and 100% of the normalized laser intensity for decay and rise times, respectively.

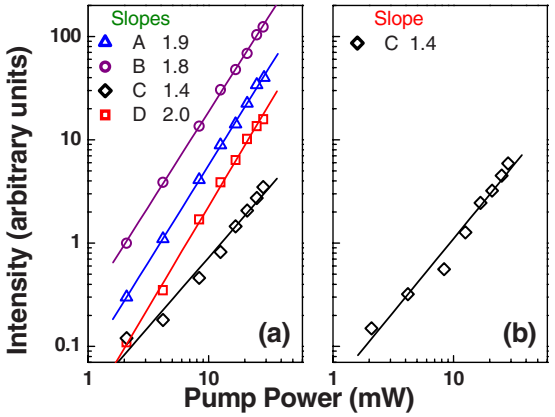

FIG. 4. (Color online) Dependence of the UC intensity with the pump power: (a) emission at 550 nm (b) emission at 650 nm.

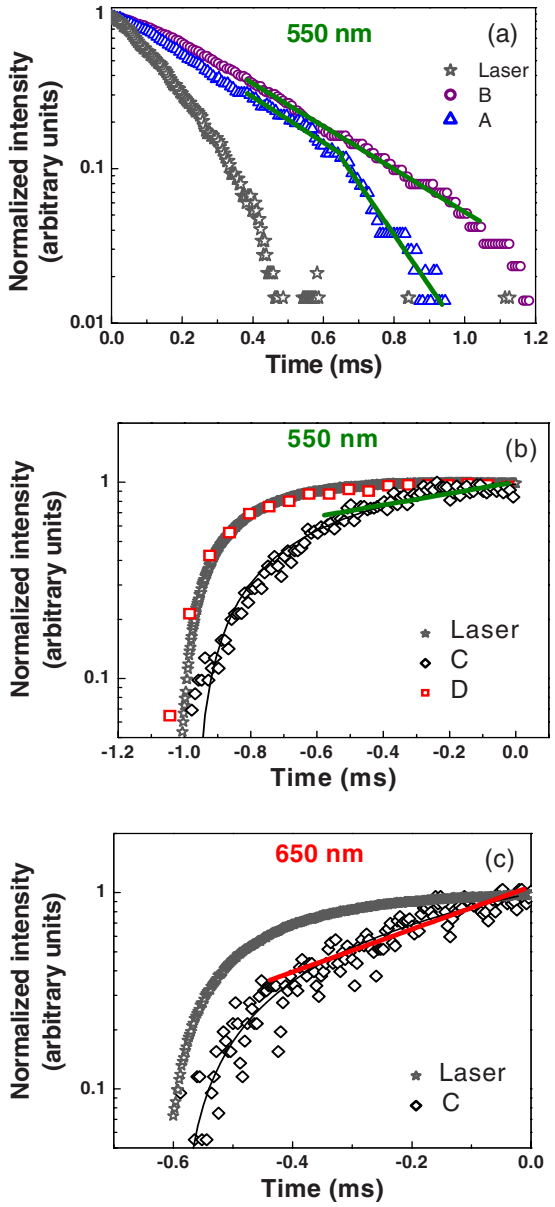

FIG. 5. (Color online) (a) Decay of the luminescence signal originated from the $^4S_{3/2}$ level (550 nm). Sample A (triangles) and sample B (circles). The scattered laser signal is represented by the stars. (b) Rise time of the 550 nm signal for samples C (diamonds) and D (squares). The dynamics is clearly limited by the temporal resolution of the apparatus in the case of sample D. (c) Rise time of the 650 nm signal for sample C.

Concerning samples A and B, the UC signal rise time given in Table II (≤ 0.18 ms) confirms that the UC pathway corresponds to two steps of one-photon absorption ($^4I_{15/2} \rightarrow {}^4I_{11/2} \rightarrow {}^4F_{7/2}$). Transition $^4I_{11/2} \rightarrow {}^4F_{7/2}$ is the so-called excited state absorption (ESA). The decay signals illustrated in Fig. 5(a) show that the characteristic decay time for sample A is smaller than that for sample B, meaning that there are two dynamical regimes for these samples. The two regimes can be understood considering the role played by the cross-relaxation (CR) corresponding to $[(^4S_{3/2} \rightarrow {}^4I_{9/2}) + (^4I_{15/2} \rightarrow {}^4I_{13/2})]$ and ET $[(^4I_{11/2} \rightarrow {}^4I_{15/2}) + (^4I_{11/2} \rightarrow {}^4S_{3/2})]$ processes. In order to describe this behavior, an appropriate rate equation model was derived as follows:

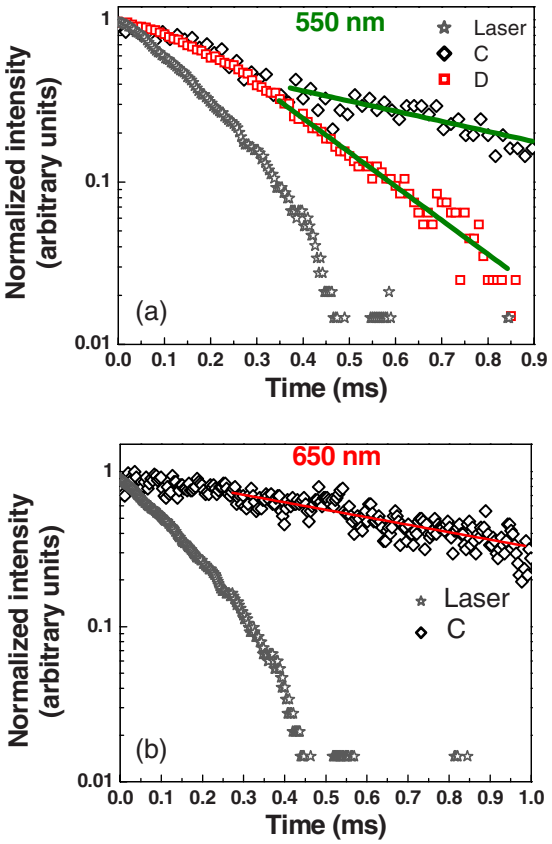

FIG. 6. (Color online) (a) Decay of the fluorescence signal at 550 nm. Sample C (diamonds) and sample D (squares). Two different regimes are observed: a fast relaxation with a characteristic time of 0.21 ms and a slow decay with characteristic time of 0.70 ms. (b) Fluorescence decay originated from the $^4F_{9/2}$ level for sample C (diamonds)—decay time: 0.90 ms.

$$\dot{n}_1 = -R_1 n_1 - W n_1 n_5 + W_1 n_3^2 + \gamma_{51} n_5 + \gamma_{41} n_4 + \gamma_{31} n_3 + \gamma_{21} n_2,$$

$$\dot{n}_2 = W n_1 n_5 + \gamma_{52} n_5 + \gamma_{42} n_4 + \gamma_{32} n_3 - \gamma_{21} n_2,$$

$$\dot{n}_3 = R_1 n_1 - R_2 n_3 - 2W_1 n_3^2 + \gamma_{53} n_5 + \gamma_{43} n_4 - (\gamma_{32} + \gamma_{31}) n_3,$$

$$\dot{n}_4 = W n_1 n_5 + \gamma_{54} n_5 - (\gamma_{43} + \gamma_{42} + \gamma_{41}) n_4,$$

$$\dot{n}_5 = R_2 n_3 - W n_1 n_5 + W_1 n_3^2 - (\gamma_{54} + \gamma_{53} + \gamma_{52} + \gamma_{51}) n_5,$$

TABLE II. Summary of the rise-times and decay times (±5%) for Er^{3+} green and red emissions.

	Emission at 550 nm		Emission at 650 nm	
Sample	Rise time (ms)	Decay time (ms)	Rise time (ms)	Decay time (ms)
A	≤0.18	Short times 0.29 Long times 0.13	···	···
B	≤0.18	0.31	···	···
C	1.48	0.70	0.40	0.90
D	≤0.18	0.21	···	···

$$n_1 + n_2 + n_3 + n_4 + n_5 = 1, \quad (1)$$

where the index $i(i=1-5)$ is related to the Er^{3+} energy levels $^4I_{15/2}$, $^4I_{13/2}$, $^4I_{11/2}$, $^4I_{9/2}$, ($^4F_{7/2}$, $^2H_{11/2}$, $^4S_{3/2}$), respectively. The pump rates are $R_i = \sigma_i I / h\nu$, where σ_i is the absorption cross section, I is the intensity of the pump laser on the sample, $h\nu$ is the photon energy, $\gamma_{i\text{-}j}(i,j=1-5)$ are the radiative plus nonradiative decay rates from level i to level j, W is the CR rate, and W_1 is the ET rate.

An analysis of the rate equation system for level 5, which originates the green emission from levels $^2H_{11/2}$ and $^4S_{3/2}$, shows the UC intensity dependence with the CR rate, ET probability and the radiative and nonradiative decay rates. A nonsteady state solution for the proposed rate equation model may describe the results shown in Fig. 5(a). However, as the set of Eqs. (1) contains the product between the populations of two distinct levels, an analytical solution is given only assuming low population of level 5, where the product $n_1 n_5 \approx n_5$. However, since this approximation is not enough to describe the luminescence signal from level 5, an analysis was made to investigate the role played by the CR, ET, and radiative and nonradiative decays for n_5. The radiative decay rate was taken from the experimental data for ZrO_2 bulk crystal and the nonradiative decay rate was estimated using the energy gap law with parameters of ZBLAN glass[20,21] that are not expect to be much different than for ZrO_2 and HfO_2. The estimated value of the total transition rate from level 5 is 1.6×10^4 s^{-1} corresponding to a decay time of 62.5 μs. Since this time is very short and does not find correspondence to the measured data, the dynamical response observed in Fig. 5(a) has to be attributed to the CR and ET. During the time interval that the chopper is blocking the laser beam, the pump rate decreases and a monoexponential decay of the luminescence is observed remaining fractions of milliseconds after the beam is blocked. As the laser wavelength is resonant with level 3, we expect that the ET process feeds efficiently level 5, even at low pump rate, and the CR removes this population efficiently. This process continues until the population of level 3 starts to decrease. In this case, ET is not an efficient channel to feed level 5 and the CR is dominant, contributing to the long decay time of the green emission. It means that that the temporal response observed in Fig. 5(a) is a competitive process between the CR and ET and depends strongly of the level 3 population.

The fluorescence spectra of ZrO_2 codoped with 1.0% Er^{3+} and 1.0% Yb^{3+} (sample C) and HfO_2 codoped with 1.0% Er^{3+} and 1.0% Yb^{3+} grains (sample D) are also shown in Fig. 2. For these two samples, weak red emission is observed at ≈650 nm. As is illustrated in Fig. 3, besides the direct absorption of two laser photons starting from the ground state ($^4I_{15/2}$) to state $^4F_{7/2}$, another mechanism contributing to the green and red emissions is the ET from an excited neighbor Yb^{3+} ion to the Er^{3+} ion. For the green emission, the process occurs in two steps. In the first step the $^4I_{11/2}$ level is populated via ground state absorption ($^4I_{15/2} + h\nu_{laser} \rightarrow {}^4I_{11/2}$) and ET via [$^2F_{5/2}(Yb^{3+}) + {}^4I_{15/2}(Er^{3+}) \rightarrow {}^2F_{7/2}(Yb^{3+}) + {}^4I_{11/2}(Er^{3+})$]. In the second step the Er^{3+} ions in the $^4I_{11/2}$ level are excited to the $^4F_{7/2}$ level via ESA ($^4I_{11/2} + h\nu_{laser} \rightarrow {}^4F_{7/2}$) and ET [$^2F_{5/2}(Yb^{3+}) + {}^4I_{11/2}(Er^{3+})$

$\rightarrow {}^2F_{7/2}(Yb^{3+}) + {}^4F_{7/2}(Er^{3+})]$. Nonradiative relaxation from the ${}^4F_{7/2}$ to ${}^2H_{11/2}$ and ${}^4S_{3/2}$, and radiative decay from those levels to the ${}^4I_{15/2}$ will give origin to the emissions centered at 525 and 550 nm. The red emission is due to the radiative relaxation from the ${}^4F_{9/2}$ to ${}^4I_{15/2}$. The ${}^4F_{9/2}$ level is populated via nonradiative relaxation from upper levels, via ESA $({}^4I_{13/2} + h\nu_{laser} \rightarrow {}^4F_{9/2})$ and ET $[{}^2F_{5/2}(Yb^{3+}) + {}^4I_{13/2}(Er^{3+}) \rightarrow {}^2F_{7/2}(Yb^{3+}) + {}^4F_{9/2}(Er^{3+})]$.

The dependence of the fluorescence intensity at 550 and 650 nm with the input power is shown in Figs. 4(a) and 4(b). Slopes of 1.4 and 2.0 for samples C and D for the green emission, and 1.4 for sample C for the red emission were obtained. These results indicate that for sample D, two photons of 980 nm are involved in the excitation of the Er^{3+} ions and the ET mechanism from Yb^{3+} is poorly efficient, that is evidenced observing the fast rise time of the ${}^4S_{3/2}$ level, as is shown in the Fig. 5(b). The decay time of 0.21 ms obtained from Fig. 6(a) is similar to the decay time obtained for sample B, then the mechanism of UC should be explained by CR and ET between Er^{3+} ions.

The behavior of sample C is different. The influence of ET from Yb^{3+} to Er^{3+} ions is clearly observed in the slopes indicated in Fig. 4 and the different rise times shown in Figs. 5(b) and 5(c). These times are 1.48 and 0.40 ms for the green and red signals, respectively, indicating that the ET process $[{}^2F_{5/2}(Yb^{3+}) + {}^4I_{11/2}(Er^{3+}) \rightarrow {}^2F_{7/2}(Yb^{3+}) + {}^4F_{7/2}(Er^{3+})]$ is more efficient than the process $[{}^2F_{5/2}(Yb^{3+}) + {}^4I_{13/2}(Er^{3+}) \rightarrow {}^2F_{7/2}(Yb^{3+}) + {}^4F_{9/2}(Er^{3+})]$. On the other hand, the temporal response of the green emission shown in Fig. 6(a) is affected by CR, ET between Er^{3+} ions, and ET between Er^{3+} and Yb^{3+} ions. The decay time of the signal from sample C is larger than for sample B, indicating that other mechanism like the ET $[{}^2F_{5/2}(Yb^{3+}) + {}^4I_{11/2}(Er^{3+}) \rightarrow {}^2F_{7/2}(Yb^{3+}) + {}^4F_{7/2}(Er^{3+})]$ is contributing to increase the population of the level 5. In order to understand the long lifetime of the level ${}^2F_{5/2}(Yb^{3+})$ we have to consider contribution from energy back-transfer as described by $[{}^4S_{3/2}(Er^{3+}) + {}^2F_{7/2}(Yb^{3+}) \rightarrow {}^4I_{13/2}(Er^{3+}) + {}^2F_{5/2}(Yb^{3+})]$.

The measured decay time of the red UC signal was 0.90 ms. The contribution of the radiative and nonradiative decay rates from the level ${}^4F_{9/2}$ was obtained following the same procedure for the level ${}^4S_{3/2}$. In this case, the total transition rate was 2.4×10^3 s^{-1}, corresponding to a decay time of 0.40 ms, indicating that the contribution of upper levels, ESA $({}^4I_{13/2} + h\nu_{laser} \rightarrow {}^4F_{9/2})$, and ET $[{}^2F_{5/2}(Yb^{3+}) + {}^4I_{13/2}(Er^{3+}) \rightarrow {}^2F_{7/2}(Yb^{3+}) + {}^4F_{9/2}(Er^{3+})]$ are important to increase the population of the level ${}^4F_{9/2}$.

A balance between the mechanisms described above is determining the temporal response shown in the Figs. 6(a) and 6(b). The slope of 1.4 observed for the green and red emissions indicates saturation of the ${}^4I_{13/2}$ level attributed to the energy back-transfer mechanism $[{}^4S_{3/2}(Er^{3+}) + {}^2F_{7/2}(Yb^{3+}) \rightarrow {}^4I_{13/2}(Er^{3+}) + {}^2F_{5/2}(Yb^{3+})]$.[22]

IV. CONCLUSIONS

The infrared-to-green and infrared-to-red frequency UC processes were studied in ZrO_2 and HfO_2 NC doped with Er^{3+} and Er^{3+}/Yb^{3+}. Red UC emission was observed only for the samples with Yb^{3+} as codopant. The decay times for ZrO_2 doped only with erbium are different due to changes in the crystal size and doping concentration. Although HfO_2 and ZrO_2 NC are isostructural, a comparison between HfO_2 and ZrO_2 NC codoped with Er^{3+}/Yb^{3+} reveals that the inclusion of Yb^{3+} strongly affects the crystalline structure and the luminescence properties in the visible spectrum of the hafnia NC. For the codoped samples studied, the hafnia matrix presents four times higher UC efficiency in the green region than zirconia, while the latter shows two times higher UC efficiency than the hafnia in the red region. However, the signal intensity in this region is ~50 times weaker than that in the green.

ACKNOWLEDGMENTS

We acknowledge the financial support from the Brazilian agencies Conselho Nacional de Desenvolvimento Científico e Tecnológico (CNPq) and Fundação de Amparo à Ciência e Tecnologia de Pernambuco (FACEPE). This work was performed under the Nanophotonics Network Project and INCT de Fotônica Project (CNPq).

[1] *Erbium-doped Fiber Amplifiers*, edited by E. Desurvire (Wiley, New York, 1994).
[2] M. Yamane and Y. Asahara, *Glasses for Photonics* (Cambridge University Press, Cambridge, 2000).
[3] T. T. Basiev, Y. V. Orlovskii, K. K. Pukhov, and F. Auzel, Laser Phys. **7**, 1139 (1997).
[4] C. B. de Araújo G. S. Maciel, L. de S. Menezes, N. Rakov, E. L. Falcão-Filho, V. A. Jerez, and Y. Messaddeq, C. R. Chim. **5**, 885 (2002).
[5] B. M. Tissue, Chem. Mater. **10**, 2837 (1998).
[6] W. Lozano B., C. B. de Araújo, C. Egalon, A. S. L. Gomes, B. J. Costa, and Y. Messaddeq, Opt. Commun. **153**, 271 (1998).
[7] L. P. Naranjo, C. B. de Araújo, O. L. Malta, P. A. S. Cruz, and L. R. P. Kassab, Appl. Phys. Lett. **87**, 241914 (2005).
[8] T. A. A. Assumpção, D. M. da Silva, L. R. P. Kassab, and C. B. de Araújo, J. Appl. Phys. **106**, 063522 (2009).
[9] T. Ohgaki, A. Higashida, K. Soga, and A. Yasumori, J. Electrochem. Soc. **154**, J163 (2007).
[10] R. Reisfeld, M. Zelner, and A. Patra, J. Alloys Compd. **300**, 147 (2000).
[11] A. Patra, C. S. Friend, R. Kapoor, and P. Prasad, J. Phys. Chem. B **106**, 1909 (2002).
[12] X. Zhao and D. Vanderbilt, Phys. Rev. B **65**, 075105 (2002).
[13] C. Carlone, Phys. Rev. B **45**, 2079 (1992).
[14] P. E. Quintard, P. Barbéris, A. P. Mirgorodsky, and T. Merle-Méjean, J. Am. Ceram. Soc. **85**, 1745 (2002).
[15] M. Mattarelli, M. Montagna, F. Rossi, C. Tosello, N. D. Afify, M. Betinelli, A. Speghini, C. Armellini, Y. Jestin, F. Rocca, and S. Gialanella, Opt. Mater. **31**, 1362 (2009).
[16] R. R. Gonçalves, G. Carturan, M. Montagna, M. Ferrari, L. Zampedri, S. Pelli, G. C. Righini, S. J. L. Ribeiro, and Y. Messaddeq, Opt. Mater. **25**, 131 (2004).
[17] T. Nishide, S. Honda, M. Matsuura, and M. Ide, Thin Solid Films **371**, 61 (2000).
[18] F. Vetrone, J. Boyer, J. A. Capobianco, A. Speghini, and M. Bettinelli, Appl. Phys. Lett. **80**, 1752 (2002).
[19] C. B. de Araújo, L. S. Menezes, G. S. Maciel, L. H. Acioli, A. S. L. Gomes, Y. Messaddeq, A. Florez, and M. A. Aegerter, Appl. Phys. Lett. **68**, 602 (1996).
[20] E. Greenberg, G. Katz, R. Reisfeld, N. Spector, R. C. Marshall, B. Bendow, and R. N. Brown, J. Chem. Phys. **77**, 4797 (1982).
[21] M. D. Shinn, W. A. Sibley, M. G. Drexhage, and R. N. Brown, Phys. Rev. B **27**, 6635 (1983).
[22] G. Chen, G. Somesfalean, Y. Liu, Z. Zhang, Q. Sun, and F. Wang, Phys. Rev. B **75**, 195204 (2007).